Available online at www.sciencedirect.com
ScienceDirect
Journal of Sound and Vibration 310 (2008) 631–649
JOURNAL OF SOUND AND VIBRATION
www.elsevier.com/locate/jsvi

Analyses of wave field from high-speed train on viaduct at shallow/deep soft grounds

H. Takemiya*

Department of Environmental and Civil Engineering, Okayama University, Tsushima Naka 3-1-1, Okayama-shi 700-8530, Japan

Accepted 20 September 2007
The peer review of this article was organized by the Guest Editor
Available online 3 December 2007

Abstract

In this paper, based on field measurements for the passage of the Shinkansen high speed trains on viaducts, the author reports the induced ground vibration features at distinctly different sites: one site is characterized by a deep soft soil and the other by a shallow soft soil both of which lie on stiff bottom. The conventional vibration assessment is normally addressed to the vibration levels based on acceleration maxima. However, in view of the vibration reception by nearby residents, firstly, a detailed investigation is attempted on the recorded time histories and on their Fourier spectra, locating the so-called low frequency vibration generation at the former site and such vibration impediment at the latter site. Then, theoretical consideration is to clarify the Shinkansen-train induced ground vibrations from a viaduct. The characterization based on the wave theory using the thin layer method reveals that, depending on the depth of surface layer, the ground-borne vibration is of significantly low frequency wave modes of dispersive propagation when it is deep or it makes the wave modes shifted towards higher frequency range when it is shallow. This finding makes an important element to better predict and assess vibration level and to develop barriers against it for mitigation.

1. Introduction

We are now deriving the benefits of high-speed trains in developed regions in the world. However, they often cause annoyances to the residents alongside when they run through developed areas and malfunctions to the vibration-sensitive equipment when they pass through high-tech industrial areas. Vibrations alongside train tracks are then becoming a more serious concern to people. The demands for adequate vibration assessments and the corresponding mitigation measures to reduce it within allowable threshold are growing.

Regarding train induced ground vibration, there are increasing numbers of papers that deal with simulations and field measurements. Some representative works are cited. For instance, train tracks on ground are modeled in different ways for different points of analyses by Sheng et al. [1]; Kaynia et al. [2], Degrande and Schillemans [3]; Takemiya and Bian [4]; Auersch [5], and Lombaert et al. [6]. The track, including rails,

*Tel./fax: +81 86 251 8146.
E-mail address: e_quakes@cc.okayama-u.ac.jp

0022-460X/$ - see front matter © 2007 Published by Elsevier Ltd.
doi:10.1016/j.jsv.2007.09.056

ballast, sleepers and embankments, and ground are the constituent elements for attention. On the other hand, train tracks on viaduct, commonly adopted in residential areas for safe train operation and effective land use, have been addressed by Yoshioka and Ashiya [7], Ju [8], and Takemiya and Bian [9]. Because of soft soil deposits near ground surface, the viaduct structures are often supported by piles. The train passage generates the so-called structural borne vibrations by exciting the eigen-vibration modes of the supporting viaducts.

Regarding environmental vibrations in Japan, along with the vibration law [10], the "Recommendation for anti-vibration measures against Shinkansen trains for urgent environmental conservation" [11] was issued by the Environmental Agency, Government of Japan for protecting the existing environments along the railways. The issue indicated a formula for evaluation only in terms of the vertical vibration acceleration level (VAL) with respect to a reference value at the border between the right-of-way and private lots. Therefore, the physical details of the environments have caused controversial arguments between train service authorities and residents. In the field measurement, the $\frac{1}{3}$-octave band frequency spectrum for the vertical component is commonly used for an overall evaluation. There are often claims by residents complaining of perceived higher levels of vibrations, while the measured value still stays below the threshold, especially, in the low frequency range. These vibrations travel a considerable distance from train track due to the ground filtering and even may lead to a significant amplification of vibration around nearby houses due to the structural resonance.

It is therefore essential to provide elaboration in the analysis of train-induced vibrations and propagation in ground; for instance, as in Refs. [12,13]. A series of impact forces act on rails at the moment when train wheels run on them, with specific time delays according to train geometry, sleeper spacing, and speed of motion. These periodic axle loads are transmitted from rails to ballast bed via pads and sleepers, and then to the underlying ground. Depending on the train speed, an inertia force can be generated that leads to the dynamic motions of the track–ground system. Under the situation where the train speed line passes through a ridge of the frequency–wave spectrum, an extraordinary large response results [4,12]. The fundamental theoretical analyses have been made by taking simple models of a stratum by Dieterman and Metrikin [14], and Takemiya and Goda [15]. The former pointed out that the group velocity of the dispersive media leads to the track resonance and the latter that the Airy phase of the group velocity concerns the predominant vibration transmission in the medium.

Recently, the author and others have measured the Shinkansen train-induced ground vibrations at different sites: one is a site of relatively deep soft ground and the other is at a site of shallow ground. At both sites, identical train tracks are elevated on an almost uniform viaduct. Based on these data, firstly, the significantly different features are interpreted regarding the frequency contents in the respective responses. Secondly, the surface ground motions due to the emitted vibrations from the viaduct foundations are analyzed by the SAWS method [16,17] to characterize the vibration transmission in ground as dispersive wave field. The generation of the "low frequency vibration" is particularly addressed at the soft site. A theoretical interpretation, with the aid of computer analysis using thin layer modeling [18], is attempted for the concerned vibration generation and transmission. Highlighted in it is the horizontal component along the viaduct that travels a substantial distance from the track and even at far distance it comes into structural response amplification. Since conventionally the vertical component is only addressed for attention, we should have an improvement on this issue for the better environmental assessment.

2. In-situ vibration measurements

Field measurements were conducted at different sites of the Shinkansen viaduct track and nearby ground as described below.

2.1. Case 1: deep surface layer

First demonstrated is a case where the vibration level is small but the vibration exposure for the neighboring residents is large. Fig. 1 shows a double-track viaduct of the Japan Shinkansen railway which consists of a series of three-span continuous girder units, supported by grouped pile foundations. The soil properties are described in Fig. 1, as estimated from the borehole test. The viaduct for investigation has a curved configuration of radius $R = 4000$ m in plan view.

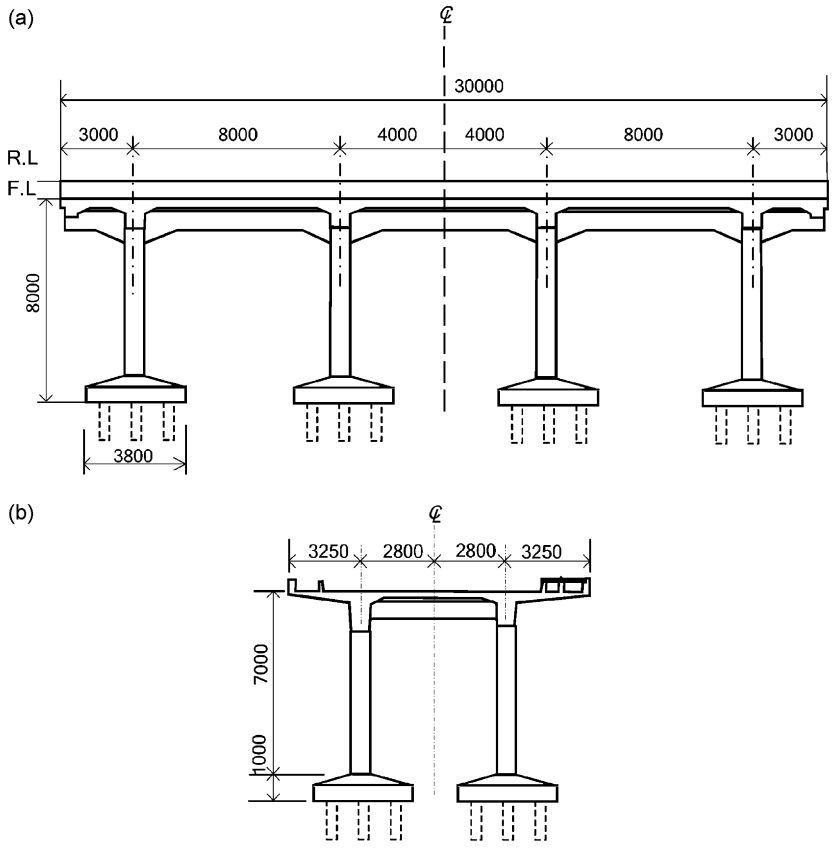

(c)

Soil properties

Layer	Thickness [m]	Density [t/m^3]	S-wave Velocity [m/s]	Poisson Ratio
1	1.0	1.5	141	0.45
2	5.5	1.6	70	0.3
3	0.5	1.7	275	0.4
4	0.5	2.0	173	0.3
5	7.5	1.7	310	0.4
6	2.0	1.8	258	0.3
7	—	1.9	320	0.3

Fig. 1. Geometry of a Shinkansen viaduct unit of a three-span continuous girder: (a) general view, (b) section view, and (c) soil properties.

The field measurement was conducted on an array transversely stretched out from a foundation of the side span of a given unit structure, as illustrated in Fig. 2. Ground observation points are positioned at intervals of 5 m outward from the viaduct, including the pillar foot. The data acquisition for the velocity response was carried out by a time increment of 0.005 s for 4096 time points by using the SPC-51D system by Tokyo Sokushin, Ltd. with servo-type VE-15D velocity sensors.

Typical response time histories are shown in Fig. 3 for acceleration, after conversion from the velocity response, for a Westbound passage of the Shinkansen "Nozomi" on the nearside track to the measurement array.

Interesting to note here is a series of impulsive-like features of short durations. They are read off around 4.8 s for the duration. In view of the train length 400 m of a 16-car Nozomi, each 25 m long, the running speed is estimated as 83.3 m/s. This confirms the train speed schedule of 300 km/h at the site. The horizontal vibration along the viaduct axis, being comparable with the vertical component in intensity, has a longer duration with a substantial tailing motion than that required for a whole train pass by a focused viaduct

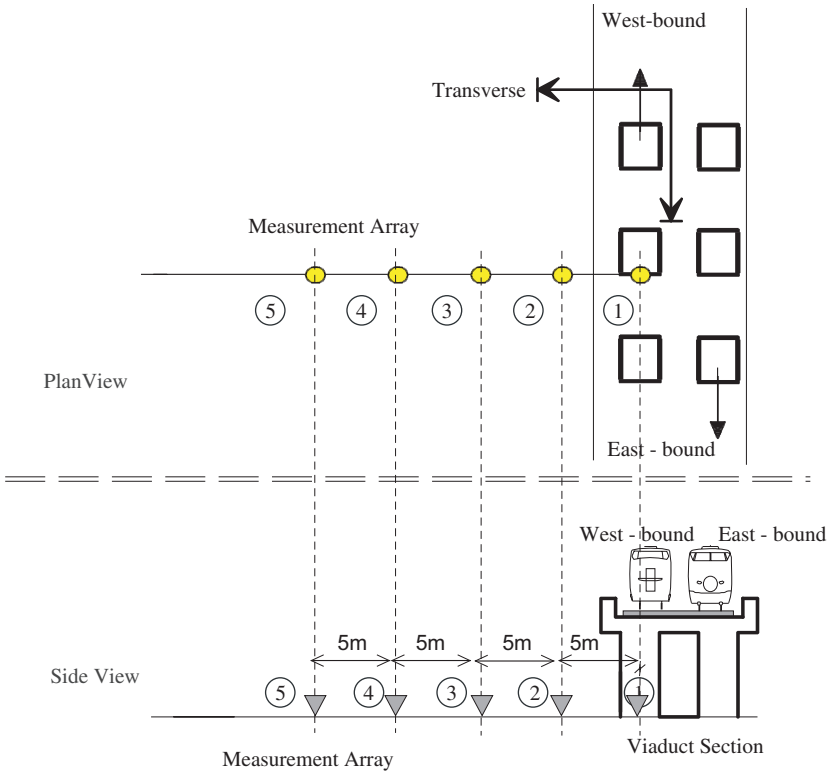

Fig. 2. In-situ measurement arrays.

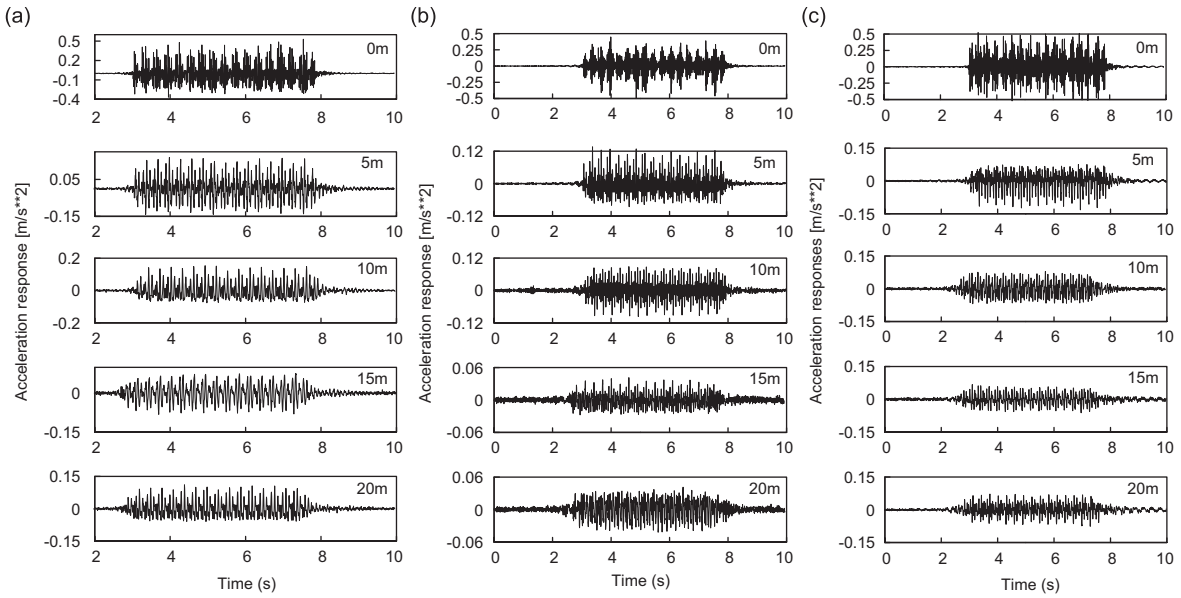

Fig. 3. Acceleration time histories of viaduct and nearby ground for a Westbound Nozomi, 300 km/h, Case 1 (a) vertical, (b) horizontal, perpendicular to viaduct, and (c) horizontal, along viaduct.

section. This indicates a free vibration of the three-span viaduct unit along the axis. The ground consequently shows similar tailing vibrations. Different responses by different track use are noticeable even for the same train. The train passage on the near track to the measurement array (on the Westbound track in this

investigation) gives rise to larger amplitudes than those on the far track (on the Eastbound track). Since the viaduct at the investigated site has the aforementioned curvature, the lateral centrifuge force exerts on the viaduct when the Shinkansen train runs there. The consequence is a substantial corresponding force action to the adjacent ground. However, as the motion is transmitted farther in ground, it becomes more subject to its filtering process through wave propagation and is attenuated geometrically.

In order to investigate the frequency contents the Fourier spectra are obtained from the time histories in Fig. 3 and depicted in Fig. 4 for the major involved frequencies up to 60 Hz at the pillar foot and up to 30 Hz at the ground. The acceleration Fourier spectra at the pillar indicate those peaks above 10 Hz are dominating frequencies In addition, the Fourier spectra of the original velocity responses are shown in Fig. 5 for comparison. These spectra reveal multiple predominant peaks at low frequencies.

If we pay attention to the velocity response at the pillar foot, the low frequency at 3 Hz appears most significantly at the viaduct in every directional component. This frequency is originated by the individual car length of 25 m at the speed of 300 km/h (83.3 ms). The viaduct–ground interaction system has a sway vibration mode also around this frequency. The correspondence between observed peak frequencies and the eigenfrequencies of the viaduct and ground system are detailed in Takemiya and Bian [9]. Other predominant peaks are located at 10, 23, 30 Hz, etc. in the vertical as well as along the viaduct axis directions but not in the horizontal transverse direction. These peaks are noted in a reverse way due to the train speed of 300 km/h (83.3 m/s) against a bogie span of 2.5 m and their arrangement distance of 4 m between adjacent cars and possibly by the viaduct individual span of 8 m.

Regarding the ground velocity response, the vertical component and horizontal transverse component have a reduced 3 Hz peak as the distance increases for observation. However, the horizontal component along the viaduct is still preserved as predominant. Therefore, the site specific wave characteristic may be pointed out as an additional cause for the 3 Hz peak. The ground velocity magnifies the above predominance. The horizontal response along the viaduct becomes comparable with the vertical component or even larger in amplitude in the low frequency range beyond a certain distance and the horizontal response perpendicular to the track becomes small.

In the Japanese vibration regulation the vibration intensity is evaluated by the acceleration level as derived by the formula

$$\mathrm{VAL} = 20\log_{10}(a_p/a_0), \tag{1}$$

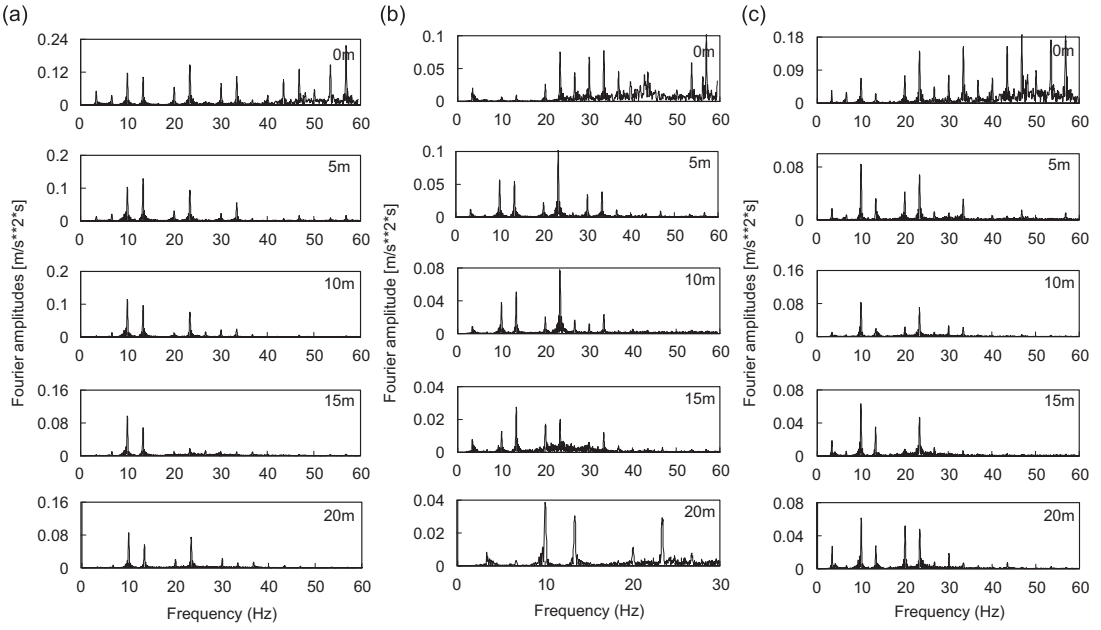

Fig. 4. Fourier spectral densities of acceleration response for a Westbound Nozomi, 300 km/h, Case 1 (a) vertical, (b) horizontal, perpendicular to viaduct, and (c) horizontal, along viaduct.

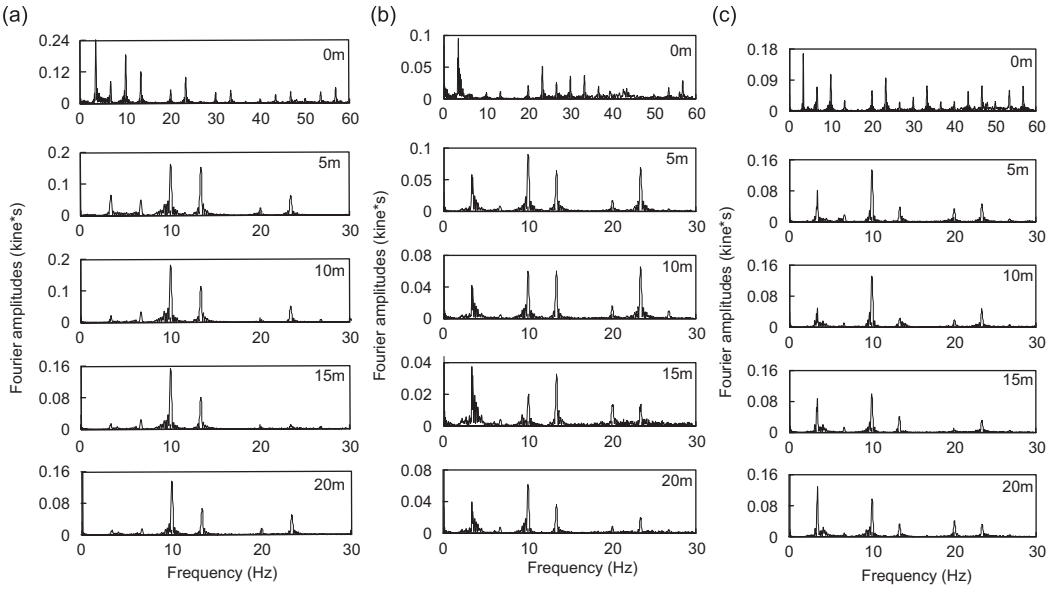

Fig. 5. Fourier spectral densities of velocity response for 300 km/h Westbound Nozomi, 300 km/h, Case 1 (a) vertical, (b) horizontal, perpendicular to viaduct, and (c) horizontal, along viaduct.

where a_p denotes an effective peak value for the acceleration time history.

$$a_{pA} = \sqrt{\frac{1}{T}\int_0^T a^2(t)\mathrm{d}t} \quad \text{with } T \text{ being the duration time of vibration} \tag{2}$$

and $a_0 = 10^{-5}[\mathrm{m/s^2}]$ is a reference value that gives rise to a threshold of 60 dB in the regulation. Eq. (2) is a gross evaluation for all the frequencies involved. The more physical frequency-dependent evaluation formula is the $\frac{1}{3}$-octave evaluation in which the effective peak values are defined for specific filtered frequency bands such that

$$a_p = \sqrt{\frac{1}{T}\int_0^T a^2(t;\, f_i \leqslant f \leqslant f_{i+1})\mathrm{d}t} \quad \text{with } T \text{ being the duration time of vibration,} \tag{3}$$

where the frequency bands are defined as

$$\frac{f_{i+1}}{f_i} = 2^{1/3} \quad \text{with a mid-frequency } f_{oi} = \sqrt{f_i f_{i+1}}. \tag{4}$$

Figs. 6 and 7 are the $\frac{1}{3}$-octave band frequency spectra to show the gross trend of the three perpendicular response components, respectively, for the Eastbound and Westbound passages of the Shinkansen Nozomi. The averaged values over the observation data on ground are drawn by the solid lines. It is noted that the directivity differences in them are small. Further, the observation data at different distances are narrowly scattered around the average value. The predominant frequencies correspond to the modal cut-off frequencies of the wave field as investigated theoretically in the next section. The lowest such frequency is taken as a cut-off frequency of the total wave propagation at the site.

The human body perception of vibrations follows the gross frequencies, not the individual frequency bands separately. Therefore, the overall evaluation over the frequencies are taken to assess the value by Eq. (1), which is alternatively given by the sum of vibration levels for each frequency band. The results are drawn in Fig. 8. The difference by the directivity of train passages seems to be small. Regarding the traffic vibration the vibration levels that incorporate a specified modification for human body perception are legitimately used. They are also plotted to refer to the environmental vibration threshold of 70 dB. Since the reduction rate by it is effective in the frequency range outside of the 4–8 Hz for the vertical response and for the frequency higher

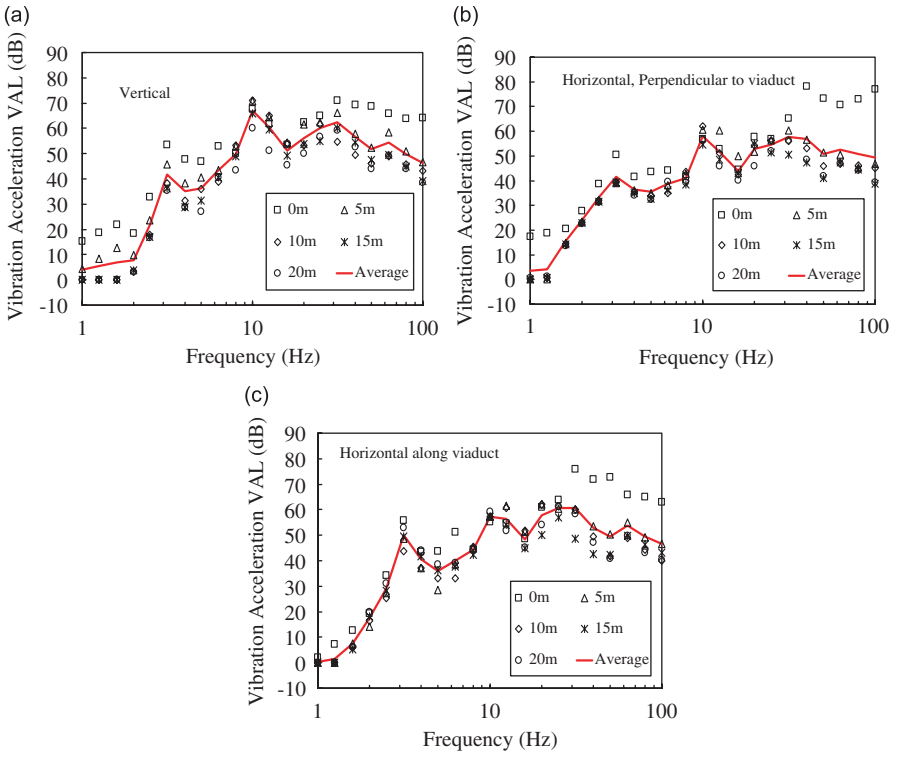

Fig. 6. The $\frac{1}{3}$-octave frequency spectra for a Eastbound Nozomi, Case 1 (a) vertical, (b) horizontal, perpendicular to viaduct, and (c) horizontal, along viaduct.

than 2 Hz for the horizontal response, then those predominant peaks in Fig. 8 are reduced accordingly in the vibration levels. The horizontal vibration level is consequently reduced more because of low frequency contents than the vertical component. However, the low frequency predominance in Case 1 may have more possibility of resonance of the neighboring houses in view of their natural frequencies. The human body perception of such amplified vibration may result in different from the above evaluation.

2.2. Case 2: shallow surface layer

Another case is demonstrated where a bigger acceleration was observed but less vibration was perceived by the alongside residents. Fig. 9 gives information about the measured viaduct that includes structural dimension, soil condition at the site, and the measurement positions. It is noted that shallow soft layers are deposited at the site. Fig. 10 shows the directly measured acceleration time histories using the same vibration sensors (Tokyo Sokushin, Ltd.) by switching the function to acceleration recording. In contrast to those in the previous investigation of Case 1, these ground motions appear in a more spindle-shaped form even at the viaduct. This may be caused by the vibration propagation in the viaduct along the axis.

Fig. 11 indicates the Fourier transforms of the time histories in Fig. 10. The vertical vibrations have almost the same frequency profile at the deck and at the footing of viaduct. In contrast to Case 1, the low frequency contents are much less included both in the viaduct and in the ground motions and almost no content in the range less than 10 Hz. Instead, there is a dominance in the frequency range 20–30 Hz. This is a consequence of a natural wave impeding effect by the shallow layers against low frequency waves below 10 Hz. For this wave cut-off phenomenon by a layer depth readers should refer to an author's publication [15,20]. The loss of frequencies higher than 30 Hz may be interpreted from the structural damping effect. The horizontal components, either along or perpendicular to the viaduct foot, have very low frequency peaks in the range less than 8 Hz at the viaduct in spite of the substantial frequencies in this range at the girder, and they disappear completely at the ground measured data.

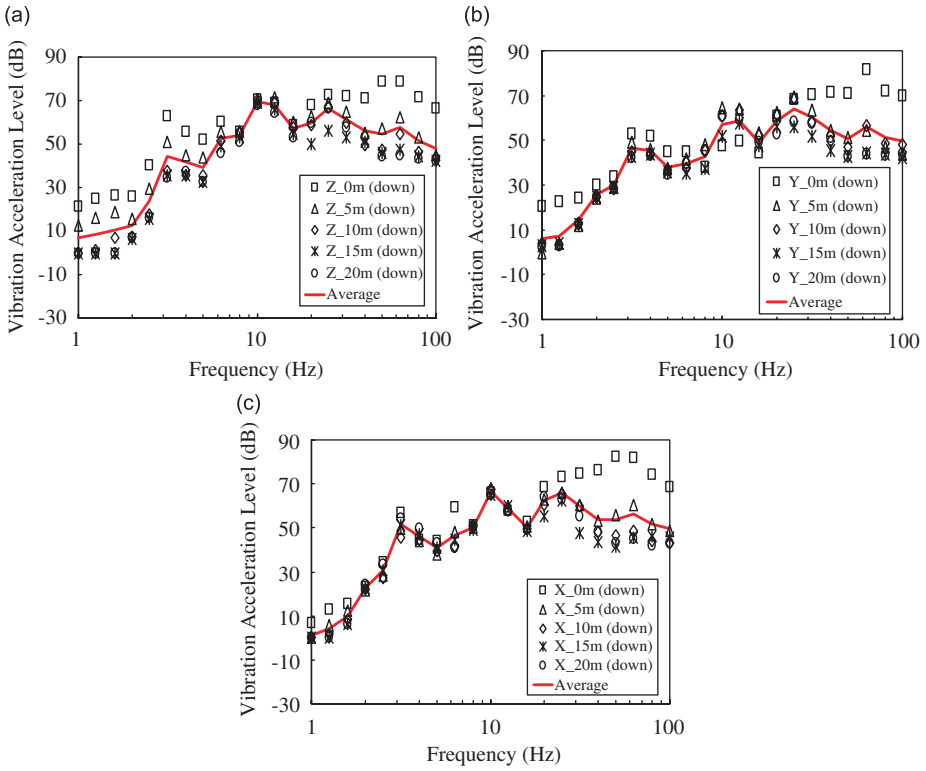

Fig. 7. The $\frac{1}{3}$-octave frequency spectra for a Westbound Nozomi, Case 1: (a) vertical, (b) horizontal, perpendicular to viaduct, and (c) horizontal, along viaduct.

Fig. 12 gives the $\frac{1}{3}$-octave band frequency spectra for all the measured distances on the ground. The averages for the respective components are depicted in the figure by the solid lines. The average value spectra for Case 1 are also depicted by the dashed lines for reference. In contrast to Case 1 where the low frequency contents around 3 Hz are predominant, Case 2 has more predominance of the higher frequencies in the range 20–30 Hz. It is noted that at 3 Hz the spectral value of Case 1 exceeds that of Case 2 in the horizontal component along the viaduct. If the same presentation is made for the velocity response, the difference becomes a more striking demonstration. The shift of the fundamental cut-off frequency toward a higher frequency to attain more predominance in this range gives a strong evidence of the significant change of vibration features. The wave cut-off effect by surface layers is noted around 8 Hz for the horizontal components whereas it is around 10–15 Hz for the vertical component.

The overall-pass vibration levels are plotted in Fig. 13 to compare with those of Case 1. In terms of maximum acceleration, Case 2 gives higher values at nearby ground to the source viaduct. The vibration acceleration values exceeding the threshold of 70 dB are noted but they are reduced within the limit once the modification by the human body perception is imposed on them. Even then, they are still higher than the corresponding values of Case 1. If we take into consideration the possibility of resonance of the neighboring residential houses, then this higher accelerations may affect them less in view of their natural frequencies.

3. Loading situation

The Shinkansen viaducts, as illustrated in Figs. 1 and 9, are categorized into an extended concrete structure, comprising consecutive three-span continuous girders supported by pillars on grouped pile foundations. Under the passages of a high-speed train the viaduct has a dynamic interaction with it and with the soil through discretely supporting foundations. The former inertia force induces not only local but also global structural vibration modes. The latter modes are more influenced by the soil condition at sites. In the previous

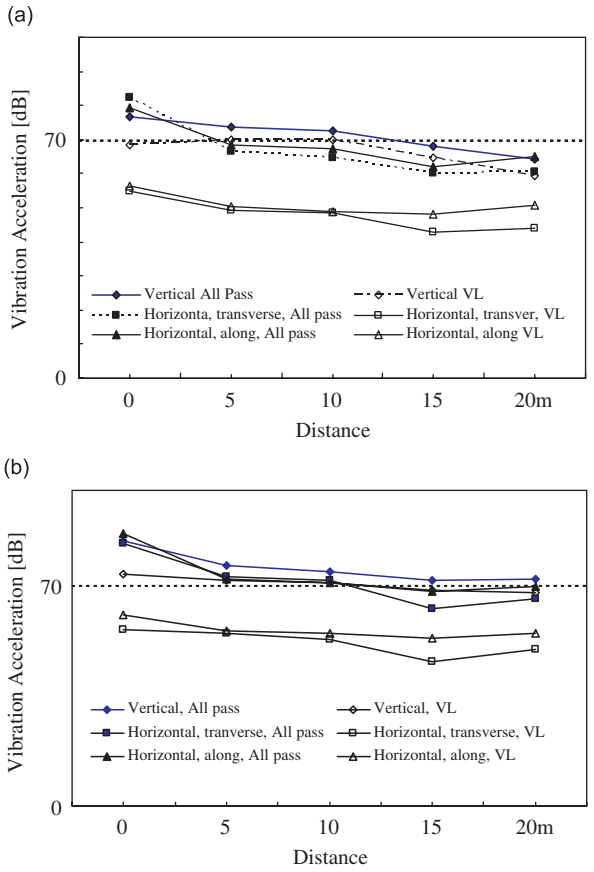

Fig. 8. Overall-pass values from the $\frac{1}{3}$-octave Fourier spectra, Case 1: (a) Eastbound Nozomi passage and (b) Westbound Nozomi passage.

paper [9], the author just assumed a direct application of moving axle loads of train on the viaduct girder. In view of a multiple supported girder by pillars, the response prediction based on the above quasi-static loading was proved acceptable from the comparison with field measured data. Regarding the loading on the ground, on the other had, considering the ratio of span length 8 m against train speed, the shifting of loading positions among foundations by the train passage should be taken into account. The emitting vibrations from multiple foundations make the wave interference in the ground according to the wave propagation speed. This is demonstrated in Ref. [9] by taking a three dimensional analysis.

Herein, in order to investigate the effect of the above shifting of wave source position on the wave field, a layered soil model that takes invariant properties along the moving direction is employed. The filtering characteristic of the ground itself does not depend on the loading condition. Therefore, the load is postulated directly on the soil surface, instead of certainly determined distribution within it along the pile depth. We further suppose a surface load distributed on a area by $F(x, y)$, moving smoothly along the y-direction with a speed c, accompanied by a harmonic oscillation of circular frequency ω_0:

$$F(x, y, z, t) = F(x, y)\delta(z)\delta(x - ct)\mathrm{e}^{\mathrm{i}\omega_0 t}, \tag{5}$$

where the notation $\delta(\,)$ stands for the Dirac's delta function and $\omega = 2\pi f$ the circular frequency with frequency f. The corresponding description of Eq. (5) in the frequency–wave number domain becomes, after the Fourier transform with respect to the space coordinates x and y, and time t, as

$$\tilde{F}(\xi_x, \xi_y, z, \omega) = \frac{2\pi}{c}\tilde{F}(\xi_x, \xi_y)\delta(z)\delta\left(\xi_y - \frac{\omega - \omega_0}{c}\right), \tag{6}$$

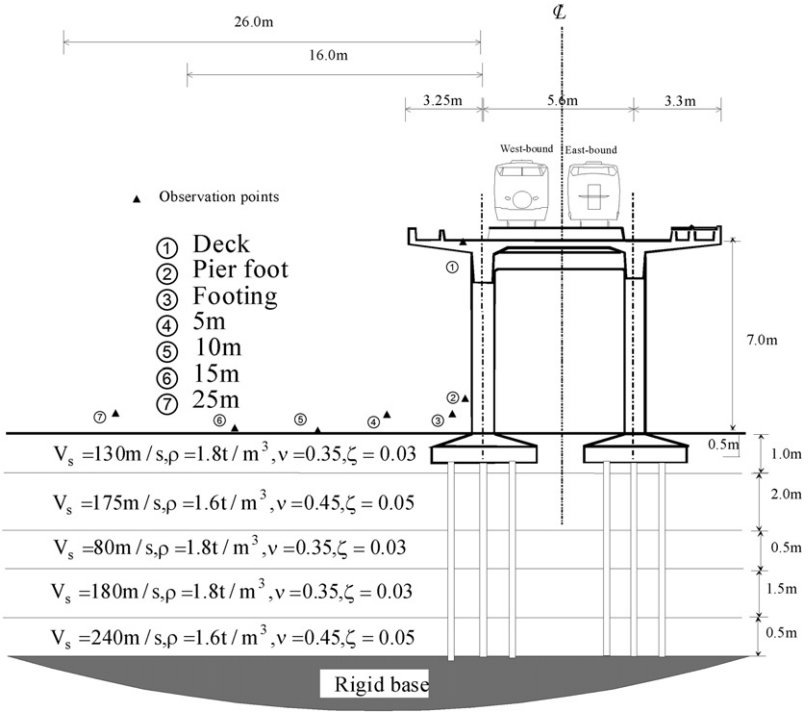

Fig. 9. Shinkansen train track on a viaduct on a shallow soft soil layers, Case 2.

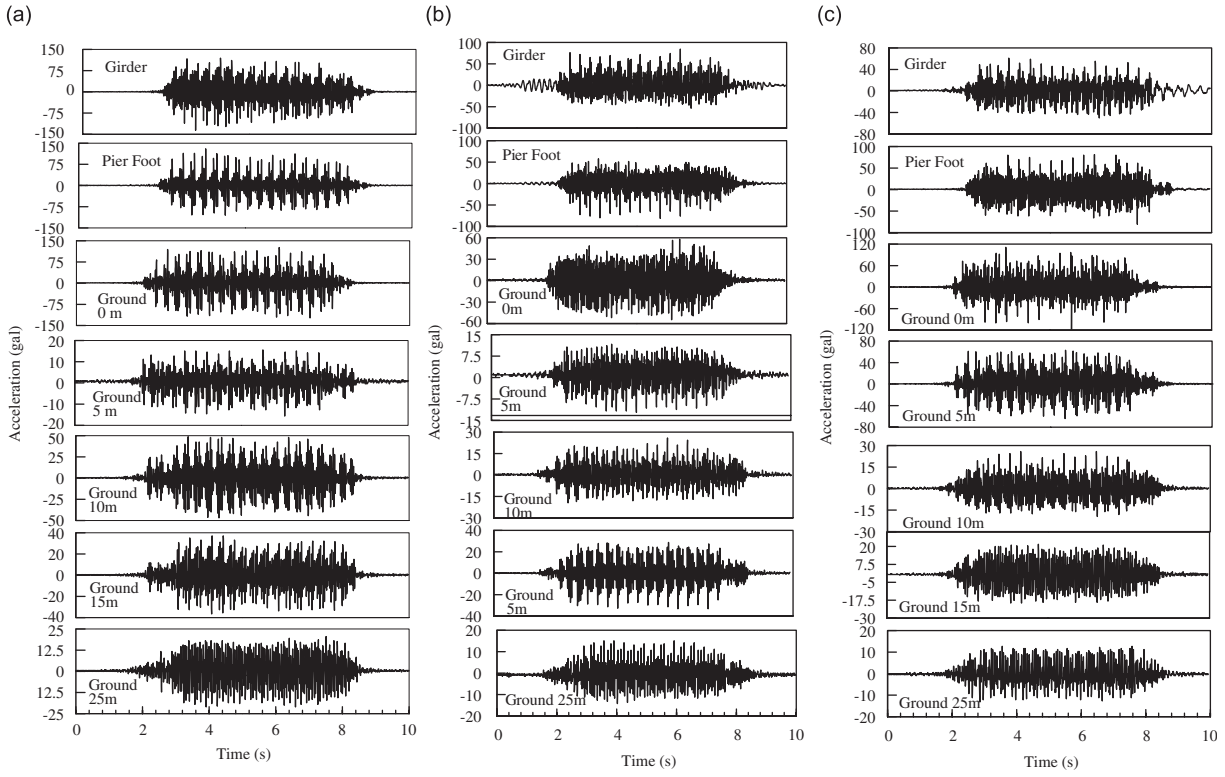

Fig. 10. Acceleration time histories of viaduct and nearby ground for a Eastbound Nozomi, 267 km/h, Case 2: (a) in-plane motion and (b) out-of-plane motion. (a) vertical, (b) horizontal, perpendicular to viaduct, and (c) horizontal, along viaduct.

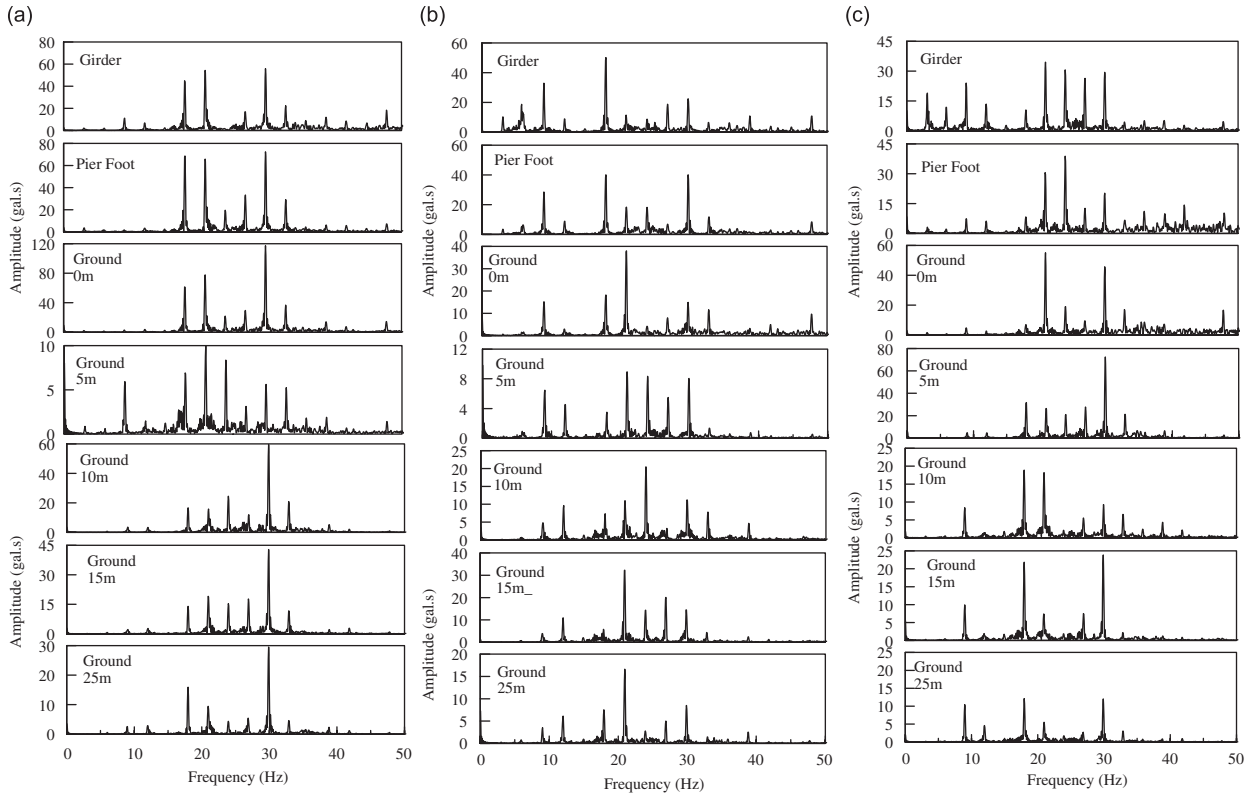

Fig. 11. Fourier amplitudes of acceleration time histories of viaduct and nearby ground for a Eastbound Nozomi, 267 km/h (a) vertical, (b) horizontal, perpendicular to viaduct, and (c) horizontal, along viaduct.

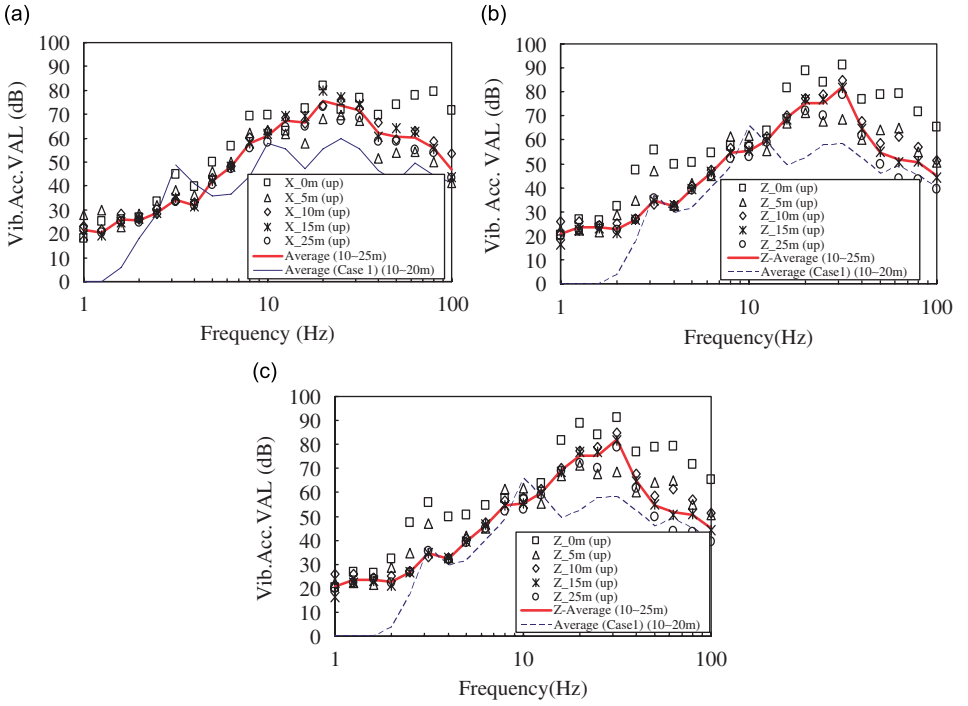

Fig. 12. The $\frac{1}{3}$-octave frequency spectra for a Eastbound Nozomi passage, 267 km/h, Case 2: (a) vertical, (b) horizontal, perpendicular to viaduct, and (c) horizontal, along viaduct.

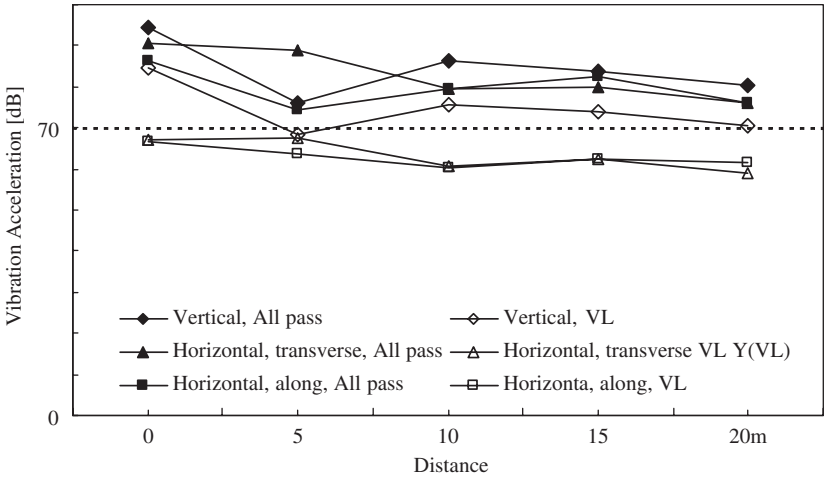

Fig. 13. Overall-pass values from the $\frac{1}{3}$-octave Fourier spectra for a Eastbound Nozomi, Case 2.

where $\tilde{F}(\xi_x, \xi_y)$ denotes the wave number domain expressions of the load intensity distribution $F(x,y)$ in x–y plane, with the ξ_x and ξ_y defining the corresponding wavenumbers. The detailed derivation and some representative load distributions are referred to Ref. [19]. The Dirac's delta function $\delta(\xi_y - (\omega - \omega_0)/c)$ describing the wavenumber in the moving direction specifies that

$$\omega = c\xi_y + \omega_0. \tag{7}$$

Once we prepare the dispersion curves that relate frequency vs. wavenumber, then Eq. (7) indicates a high concentration of the induced wave propagation energy along this line. The author has given a more detailed interpretation in Ref. [12] in terms of the wavenumber–frequency spectral density depiction.

Now we interpret the three dimensional wave field by decoupling it into the in-plane motion comprising the P and SV waves and the out-of-plane motion comprising the SH wave. The vertical and horizontal motions in the vertical plane in the transversal direction to the viaduct, if the distance is limited to the neighborhood, may be taken approximately as the in-plane motion. On the other hand, the horizontal motion parallel to the viaduct on it may be taken as the out-of-plane motion. The theoretical discussion in the next section is made on this postulation.

4. Wave field analyses

4.1. Case: deep surface layer

In order to investigate the nearby field of the viaduct under the train passage, we took a spectral analysis by applying the SASW method to the field measured data [16,17]. The ground velocity or acceleration records y_i and y_j at selected pairs of points on a measurement line are employed to predict the surface wave speed V_S traveling between these distances d_i and $d_j(\geqslant d_i)$ at a given frequency f in an elapsed time $t(f)$. Then,

$$V_S = (d_j - d_i)/t(f), \tag{8}$$

$$t(f) = \theta(f)/2\pi f, \tag{9}$$

where the phase angle $\theta(f)$:$-\pi \leqslant \theta \leqslant \pi$ is obtained from the cross-spectra of $\langle y_i y_j \rangle$ of the recorded response time histories, as

$$\theta(f) = \tan^{-1}[(\mathrm{Im}\langle y_1 y_2 \rangle)/\mathrm{Re}(\langle y_1 y_2 \rangle)]. \tag{10}$$

However, the phase angle should be appropriately counted in view of periodic shifting by $2n\pi$:

$$\theta(f) : -\pi + 2n\pi \leqslant \theta \leqslant \pi + 2n\pi. \tag{11}$$

The wavelength is then determined by

$$\lambda(f) = V_c/2\pi f. \tag{12}$$

Based on the measured velocity data for the Shinkansen train passages, thus obtained phase velocities vs. frequency is depicted in Figs. 14(a) and 15(a). In these figures the results for other types of source loadings such as impulses by a hammer and ambient motions are also plotted. The symbols indicated as "In-plane motion" are computed from the vertical response component on the transversal line to the viaduct axis. Those indicated as "Out-of-plane" are obtained from the horizontal response component parallel to the viaduct axis. Although the wave emissions are successively carried out from a multiple source locations, the in-plane is here related largely to the generalized Rayleigh-wave propagation, whereas the out-of-plane motion is to the generalized Love-wave propagation.

In order to facilitate a theoretical interpretation of wave generation and propagation in soil, the relationship of frequency vs. wavenumber is obtained by applying the thin layer procedure [18], presuming a layered soil profile in the table in Fig. 1, based on the *N*-value field test. We apply discretization by sublayers of the original soil layers so as to take a linear variation of soil deformation within each sublayer. At the same time we expand the horizontal wave propagation into the wavenumber domain via Fourier transform with respect to space and time. Then, through an appropriate transformation of coordinates we get the polarized equations for the *SV*- and *P*-wave field and for the *SH*-wave field, with the associated respective wavenumbers ξ. They are described in the transformed wavenumber domain as

$$(\mathbf{A}^{\mathrm{P-SV}}\xi^2 + \mathbf{B}^{\mathrm{P-SV}}\xi + \mathbf{C}^{\mathrm{P-SV}} - \omega^2\mathbf{M}^{\mathrm{P-SV}})\tilde{\tilde{\mathbf{U}}}_{123}^{\mathrm{P-SV}} = \tilde{\tilde{\mathbf{P}}}_{123}^{\mathrm{P-SV}}, \tag{13}$$

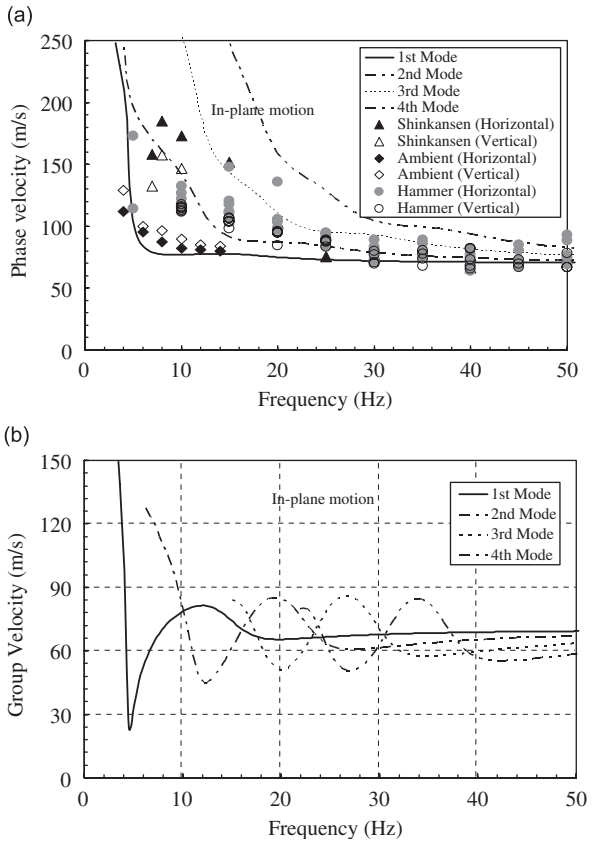

Fig. 14. Dispersive wave characteristics for in-plane motion, Case 1: (a) phase velocity vs. frequency and (b) group velocity vs. frequency.

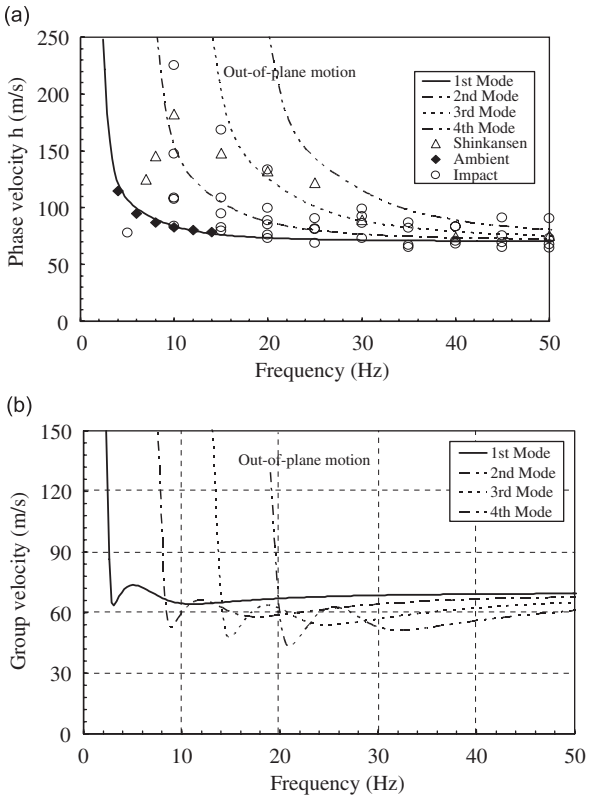

Fig. 15. Dispersive wave characteristics for out-of-plane motion, Case 1: (a) phase velocity vs. frequency and (b) group velocity vs. frequency.

$$(\mathbf{A}^{\mathrm{SH}}\xi^2 + \mathbf{C}^{\mathrm{SH}} - \omega^2\mathbf{M}^{\mathrm{SH}})\tilde{\tilde{\mathbf{U}}}^{\mathrm{SH}}_{123} = \tilde{\tilde{\mathbf{P}}}^{\mathrm{SH}}_{123}, \tag{14}$$

where $\tilde{\tilde{\mathbf{U}}}_{123}$ denotes the nodal displacement vector under a given load vector $\tilde{\tilde{\mathbf{P}}}_{123}$ in the wavenumber domain. The superscripts $SV{-}P$ and SH indicate the concerned wave field. The details of the involved matrices **A**, **B**, **C**, and **M** are determined appropriately from the soil properties and can be referred to in the original paper. The homogeneous equations of Eqs. (13) and (14), given the frequency ω, derive the wavenumbers ξ and then wave velocity V_S of the generalized surface waves.

$$V_S = \frac{\omega}{2\pi\xi} = \frac{f}{\xi} \tag{15}$$

The detail description is given in Ref. [19].

As a numerical model, in view of short wavelengths in high frequencies the minimum layer thick is determined to fulfill the wave propagation of the targeted shortest wavelength, while in view of long wavelengths in low frequencies an extended base layer is additionally put below the original surface layers. This thickness is determined by checking the prescribed phase velocity of the input shear wave at zero frequency. Herein an fixed bottom is set to the depth at 50 m. The resultant eigenvalue curves are depicted in Figs. 14(a) and 15(a) for the in-plane as well as for the out-of-plane motion. They are referred to as the first, second, third, and fourth modes in the order of wavelengths from long to short. Regarding these mode characteristics, it is interesting to note that in the frequency range below 10 Hz the measured in-plane data from the Shinkansen train fall on/near the first mode to the second mode curves and transfer from the first to the second mode occurs with increasing frequency. The out-of-plane motion indicates that the higher modes are more concerned in the response than in the in-plane motion.

Based on the phase velocity, the group velocity defined by

$$V_g = 2\pi \frac{\mathrm{d}f}{\mathrm{d}\,\xi} \approx 2\pi \frac{\Delta f}{\Delta \xi} \tag{16}$$

determines an Airy phase frequency as the local minima of the group velocity. At this frequency the majority of the wave energy is conveyed; therefore, the wave propagation/non-propagation can be demarcated by such lowest frequency, giving a vague cut-off frequency. The group velocities for different modes are depicted in Figs. 14(b) and 15(b) for which the frequency increment is used as $\Delta f = 0.05$ Hz. The Airy phase frequencies are noted approximately as 4.5 Hz for the first mode and 13 Hz for the second mode for the in-plane motion. They are 3 Hz for the first mode and 9 Hz of the second mode for the out-of-plane motion. These Airy phase frequencies lead us to better understand the ground-borne vibration.

In order to investigate the effect of the moving speed of a train on field wave generation, we recall Eq. (7). The quotient of the phase velocity against the wavenumber gives a velocity unit so that some representative train speed lines are drawn in the same dimensions to predict possible wave generation. Considering the train–track–viaduct interaction, the loading on the ground may reasonably be approximated by a moving harmonic load, although the position of the vibration emission is only limited to viaduct foundations.

In Fig. 16 the harmonic frequencies of $f_0 = 3$, 6, and 10 Hz, besides $f_0 = 0$, are chosen for the parameters. The last speed line corresponds to a smooth moving load and other speed lines to moving loads accompanied by a harmonic oscillations. These frequencies are chosen, in view of Figs. 4 and 5, to consider the predominant source and structural-borne vibrations under the train passages.

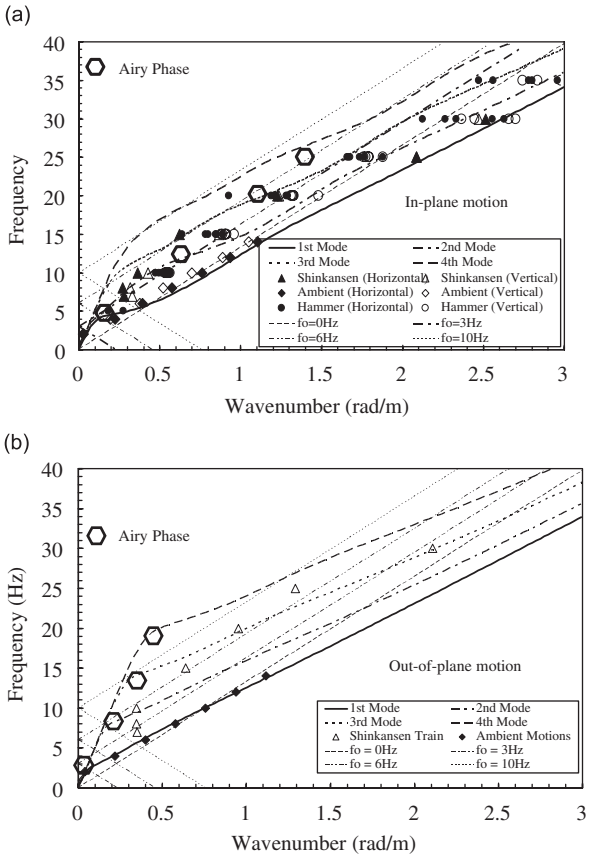

Fig. 16. Wave dispersion characteristic; frequency vs. wavenumber, Case 1: (a) in-plane motion and (b) out-of -plane motion.

Firstly, we address the ground vibration induction by the moving speed of trains. Crossings of the speed lines with the modal wave characteristic curves lead to significant vibration emission from the source into the ground. Regarding the in-plane motion, under the smooth motion of $f_0 = 0$, they are read off as 7 Hz for the first mode and 25 Hz for the second mode; under the driving frequency of $f_0 = 3$ Hz, they are 6 and 13 Hz for the second mode On the other hand, regarding the out-of-plane motion, under the smooth motion of $f_0 = 0$, they are read off as 10 Hz for the first mode and 22 Hz for the second mode; under the driving frequency of $f_0 = 3$ Hz, they are 4 and 15 Hz both for the second mode. Some of the above specific frequencies relate the peak frequencies in Figs. 4 and 5 at the foundation and the neighboring ground.

Secondly, we investigate the ground transmissibility of vibration under the emitting vibration from the source location. This defines an incoming or "imission" problem to vibration receivers. In the in-plane motion for the viaduct transverse section, the lowest Airy phase frequency, marked by a hexagon symbol ⬡, is close to the crossing frequency of the speed line of $f_0 = 3$ Hz with the first mode curve. In fact, this wave mode approaches the second mode closely in this frequency range. The second mode Airy phase is almost the same frequency of this speed line crossing with the second mode curve. Therefore, the first mode is expected to dominate the response in the former situation whereas the second mode dominates in the latter situation. The contributions of the higher modes are generally small. In the out-of-plane motion for the viaduct transverse section, the Airy phase of the first mode is located at 3 Hz but the speed line crossing frequencies with most of the depicted modes are higher than this frequency. The Airy phase of the second mode is located off the speed line crossing with the wave mode curves. Therefore, the response amplification around 3 and 10 Hz may be attributed to the Airy phase propagation of the SH waves, in addition to wave generation by the speed line crossing of $f_0 = 0$ with the first wave mode at the latter frequency. These interpretations prove an observation that the low frequency motion along the viaduct gets larger than the transversal motion with increasing distance of a focused point.

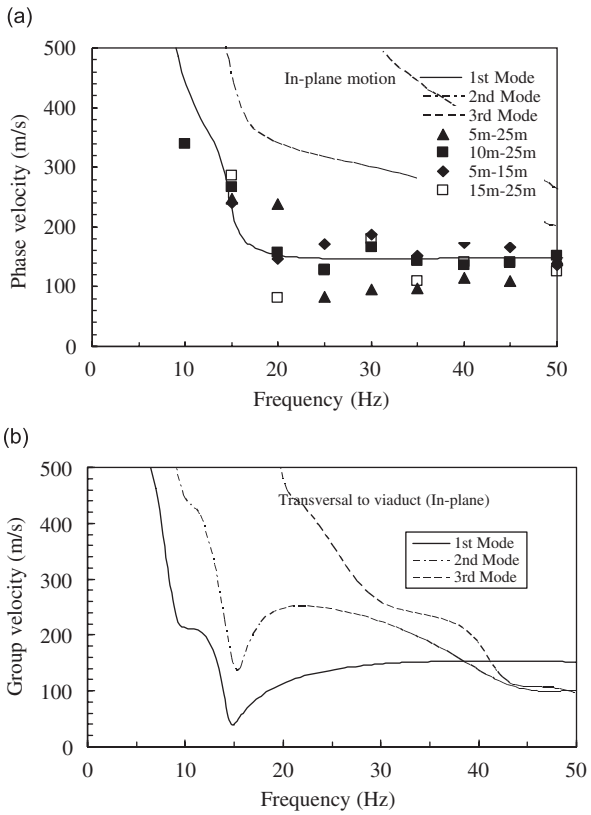

Fig. 17. Dispersive wave characteristics for in-plane motion, Case 2: (a) phase velocity vs. frequency and (b) group velocity vs. frequency.

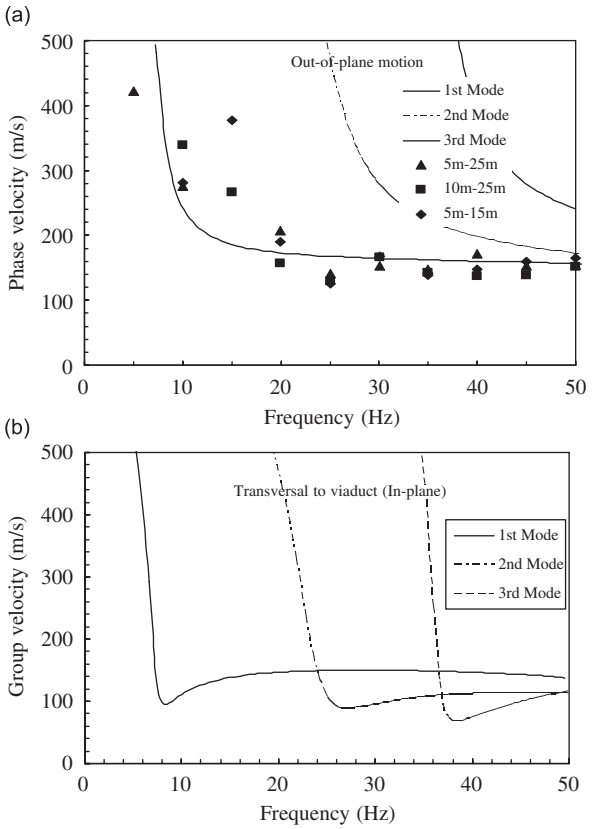

Fig. 18. Dispersive wave characteristics for out-of -plane motion, Case 2: (a) phase velocity vs. frequency and (b) group velocity vs. frequency.

4.2. Case 2: shallow surface layer

The wave dispersion characteristics are investigated based on the soil properties in Fig. 9. The dispersion curves of the phase velocity vs. frequency and the group velocity vs. frequency are depicted in Fig. 17 for the in-plane motion and in Fig. 18 for the out-of-plane motion. The Airy phase for the in-plane motion is clearly identified from the group velocity at 15 Hz for both the first and second modes. For the out-of-plane motion they exist at 8 Hz for the first mode and at 26 Hz for the second mode. The dispersion characteristic is investigated in Fig. 19 in the relation of frequency vs. wavenumber. The measured acceleration data for the Shinkansen passage are also analyzed by the SASW method and plotted in the same figure for comparison. Crossings of the speed lines with the modal wave characteristic curves are interpreted. The harmonic driving frequencies are again taken as $f_0 = 0$, 3, 10, and 30 Hz in view of the peak frequencies at the foundation in Fig. 11. Regarding the in-plane motion, only under the driving frequency of $f_0 = 3$ Hz, the crossing is noted at 15–20 Hz for the first mode; under other driving frequencies no crossing occurs. On the other hand, regarding the out-of-plane motion, under the driving frequency of $f_0 = 10$ Hz, it is read off as 17 Hz only for the first mode; under the driving frequency of $f_0 = 30$ Hz, it occurs at higher frequency than 50 Hz. The field measured data mostly scatter around the first wave mode.

The vibration emission from train passages and ground transmissibility is predicted in view of the Airy phase frequency and the crossing frequency of the speed lines with the modal wave dispersion curves. The lowest Airy phase frequency at 8 Hz for the in-plane motion falls roughly on the fundamental wave mode cut-off frequency. The crossing of the speed line with modal wave dispersion curves proves the peak response at 15–20 Hz. Therefore, the ground vibration in Case 2 is characterized by the high frequency contents and they result in the high vibration level in Fig. 12 consequently.

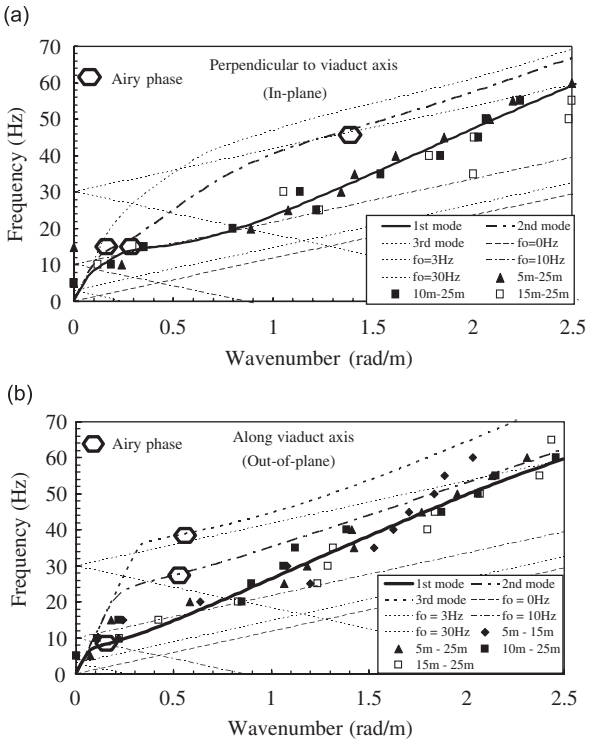

Fig. 19. Wave dispersion characteristic; frequency vs. wavenumber, Case 2: (a) in-plane motion and (b) out-of -plane motion.

5. Conclusion

Based on the measured data at distinctly different site conditions, the train induced wave fields have been analyzed with attention to the frequency contents, besides the vibration intensity. The theoretical interpretation is attempted with due consideration of the dispersion characteristics from the thin layer approach.

The findings are summarized as follows:

(1) In the case of train passage on viaduct, although the source loading generates a wide range of frequencies, the global vibration eigenmodes of a viaduct is more dominating the response in interaction with soil.
(2) The ground response at nearby viaduct due to high-speed train passage on it is changed drastically by the site conditions, especially by the depth of the soft surface layer; even though the viaduct and train loads are almost the same. The wave propagation or the cut-off phenomenon is clearly observed in the measured ground data once we take the $\frac{1}{3}$-octave band frequency spectra. In the Case 1 study, the first Airy phase frequency exists at low frequency whilst in the Case 2 study it is shifted to the higher frequency.
(3) The low frequency vibration that is caused by the global viaduct behavior along its axis is significantly transmitted toward far distances. In the investigated cases herein, the transmission is higher for the horizontal motion, possibly by a SH wave propagation, than other component motions. This may suggest that the current regulations that pay attention exclusively to the vertical component should be amended in view of even its possible amplification by residential houses.
(4) The vibration assessment has been carried out in terms of the observed maximum acceleration. However, the predominance of low frequency contents is most crucial from the viewpoint of human body perception. The velocity evaluation may be a better indicator in this sense than acceleration.
(5) Passages of the Shinkansen trains generate the vibration frequencies not only by the train geometry against its speed at source, but also by the viaduct structural vibration modes due to the inertia they create with the supporting soil.

(6) Besides the Airy phase frequencies in ground wave field, the crossing of the speed lines with the dispersion curves generates significant wave propagation. In the Case 1 study the former is a primary cause for the wave field, whereas in the Case 2 study the latter dominates the wave field.
(7) In order to predict the wave field to be generated by train passages, certainly specified harmonic moving surface loads on the focused layered soil may suffice to establish the relevant relationship of frequency vs. wavenumber.

Acknowledgment

The author expresses sincere gratitude to Dr. Jorge Shimabuku, Kozo Keikaku Kenkyusho for a part of computation involved herein.

References

[1] X. Sheng, C.J.C. Jones, M. Petyt, Ground vibration generated by a harmonic load acting on a railway track, *Journal of Sound and Vibration* 225 (1) (1999) 3–28.
[2] A.M. Kaynia, C. Madshus, P. Zackrisson, Ground vibration from high-speed trains: prediction and countermeasure, *Journal of Geotechnical and Geoenvironmental Engineering, ASCE* 126 (6) (2000) 531–537.
[3] G. Degrande, L. Schillemans, Free field vibrations during the passage of a Thalys high-speed train at variable speed, *Journal of Sound and Vibration* 247 (1) (2001) 131–144.
[4] H. Takemiya, X.C. Bian, Substructure simulation for train track/layered ground interaction dynamics through discrete sleepers, *Journal of Engineering Mechanics Division, ASCE* 131 (7) (2005) 699–711.
[5] L. Auersch, The excitation of ground vibration by rail traffic: theory of vehicle–track–soil interaction and measurements on high-speed lines, *Journal of Sound and Vibration* 284 (2005) 103–132.
[6] G. Lombaert, G. Degrande, J. Kogut, S. François, The experimental validation of a numerical model for the prediction of railway induced vibrations, *Journal of Sound and Vibration* 6 (2006) 512–535.
[7] A. Yoshioka, K. Ashiya, A dynamic model on excitation and propagation of Shinkansen-induced ground vibrations, *Butsuri-Tansa* 48 (5) (1995) 299–315.
[8] S.H. Ju, Finite element analyses of wave propagations due to a high-speed train across bridges, *International Journal for Numerical Methods in Engineering* 54 (2002) 1391–1408.
[9] H. Takemiya, X.C. Bian, Shinkansen high-speed train Induced ground vibrations in view of viaduct–ground interaction, *Soil Dynamics and Earthquake Engineering* 27 (2007) 506–520.
[10] Vibration Regulation Law, Ministry of Environment, Government of Japan, 1976.
[11] Environmental Agency, Government of Japan, Recommendation for anti-vibration measures against Shinkansen trains for urgent environmental conservation, 1976.
[12] H. Takemiya, Simulation of track-ground vibrations due to a high-speed train: the case of X-2000 at Ledsgard, *Journal of Sound and Vibration* 261 (3) (2003) 503–526.
[13] H. Takemiya, X.C. Bian, K. Yamamoto, T. Asayama, High speed train induced ground vibrations: transmission and mitigation for viaduct case, *Proceedings of the Eighth International Workshop on Railway Noise*, ISVR, Vol. 1, 2004, pp. 107–118.
[14] H.A. Dieterman, A.V. Metrikine, Critical velocities of a harmonic load moving uniformly along an elastic layer, *Transactions of the ASME Journal of Applied Mechanics* 64 (1997) 596–600.
[15] H. Takemiya, K. Goda, Wave propagation/impediment in a soil stratum over rigid base due to impulse/moving loads, *Proceedings of the Japan Society of Civil Engineers*, Vol. 605/I-45, 1998, pp. 161–169.
[16] N. Gucunski, R.D. Woods, Numerical simulation of the SASW test, *Soil Dynamics and Earthquake Engineering* 11 (1992) 213–227.
[17] K.H. Stokoe, S.G. Wright, J.A. Bay, J.M. Roesset, Characterization of geotechnical sites by SASW method, ISSMFE, Vol. TC♯10, 1994, pp. 15–25.
[18] E. Kausel, An explicit solution for the Green functions for dynamic loads in layered media, Research Report R81-13, MIT, 1981.
[19] H. Takemiya, Ground vibrations alongside tracks induced by high-speed trains: prediction and mitigation, in: V.V. Krylov (Ed.), *Noise and Vibration from High-speed Trains*, Thomas Telford, 2001, pp. 347–393.
[20] H. Takemiya, A. Fujiwara, Wave propagation/ impediment in a stratum and wave impeding block (WIB) measured for SSI response reduction, Hirokazu, *Soil Dynamics and Earthquake Engineering* 13 (1994) 49–61.